Chapter 5

5. SELECTIVE ADSORPTION OF DYE POLLUTANTS FROM THEIR MIXTURE USING SnO_2 NANOSTRUCTURES

In this chapter of the thesis, we have discussed the results of selective adsorption of two tin dioxide (SnO_2 NP and SnO_2 NS) nanostructures synthesized via a simple template-free solvothermal route. The results of activity measurement of the nanostructures toward the selective adsorption of organic dye pollutants such as Congo red (CR) and rhodamine B (RhB) from their mixed aqueous solution have been discussed. Figure 5.1 represents the molecular structure of the respective dyes, viz., Congo red and rhodamine B.

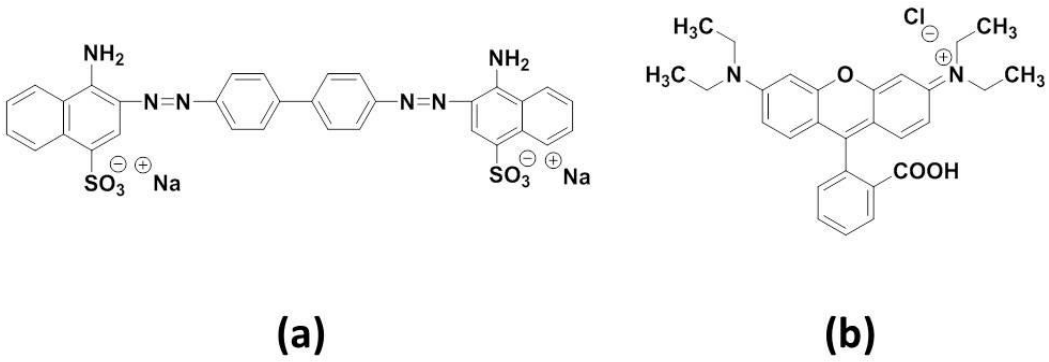

Figure 5.1 Molecular structures of (a) Congo red and (b) Rhodamine B.

5.1 Prologue

Water is essential for all living things to exist. However, pollution of aquatic environment by various contaminants over the decades has led to a serious global problem. Therefore, researchers have focused on the treatment of such water contaminants [1, 2]. In this context, dye represents a common polluting substance that has gradually become the major source of water pollution [3, 4]. Concomitantly, the demand for such dyes has been increasing in various industries such as textiles, leather, cosmetics and so forth [4, 5]. Therefore, removal of dye contaminants from wastewater before disposal into water bodies has become a critical issue [2]. Different treatment technologies that have been developed so far for the removal of dye pollutants include adsorption, photodegradation, reduction, membrane filtration, chemical coagulation and so on [6–9]. However, owing to its simplicity and high efficiency with no secondary pollution, adsorption is the most preferred approach among others [10–12]. Hence, significant effort has been made by researchers to find out new adsorbent materials with

better efficiency. Among the various adsorbents, activated carbon is one of the most effective adsorbents for purification of wastewater owing to its significantly high surface area and porous nature [12–14]. However, certain limitations associated with this material are high cost, complex and expensive synthesis procedure and long removal time with low selectivity which make it economically infeasible [15]. To overcome these limitations, it is essential to prepare other cost-effective materials having high selectivity. Hence, SnO_2 nanostructures with different morphologies are employed for selective adsorption of such organic dye pollutants. The details on the properties of SnO_2 are briefly described in Chapter 1. Also, the synthetic procedures for the SnO_2 nanostructures and their characterization techniques are described in Chapter 2.

5.2 Results and discussion

5.2.1 Characterization

The complete characterizations of the SnO_2 nanostructures, viz., SnO_2 NP and SnO_2 NS are described in Section 3B and 3C of Chapter 3, respectively.

5.2.2 Selective adsorption study by SnO_2 nanostructures

5.2.2.1 Effect of contact time

The adsorption equilibrium studies for the mixture of the dyes, Congo red (CR) and rhodamine B (RhB) are carried out at room temperature at pH 3.0 and 7.0, respectively. The effect of contact time is investigated in order to identify the minimum time needed for adsorption to attain steady state. As shown in Figure 5.2, the adsorption capacities of the SnO_2 nanostructures increase rapidly within the first 20 min and then proceed slowly until the steady state is reached within 60 min, indicating very quick adsorption of both the dyes onto the SnO_2 surfaces. After 60 min, the value of adsorption capacity, q_e did not change. Therefore, 60 min is determined as the contact time for further adsorption studies of the mixture of both dyes. At pH 3.0, the values of q_e for the adsorption of CR are 15.40 and 12.80 mgg^{-1}, whereas at pH 7.0 the values are 13.27 and 11.40 mgg^{-1} due to the adsorption of RhB onto SnO_2 NS and SnO_2 NP, respectively. The results show that the SnO_2 NS exhibit higher adsorption activities than SnO_2 NP for the adsorption of both dyes, indicating SnO_2 NS as a better adsorbent material.

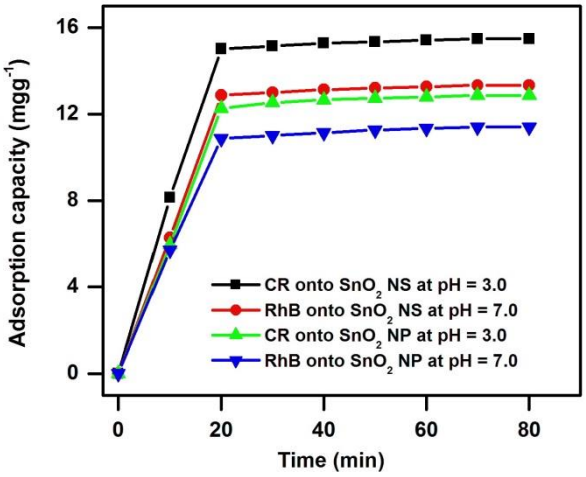

Figure 5.2 Effect of contact time on adsorption capacity at pH 3.0 & 7.0 at 497 & 554 nm onto SnO_2 nanostructures for CR and RhB, respectively. Conditions: amount of mixed dye solution = 20 mL, concentration of dye solution = 3 mgL^{-1} and amount of catalyst = 3 mg.

5.2.2.2 Adsorption kinetics

To investigate the adsorption kinetics of CR and RhB on the SnO_2 nanostructures, two conventional kinetic models, viz., pseudo-first order and pseudo-second order kinetic models, are applied. The pseudo-first order (equation 5.1) and pseudo-second order (equation 5.2) kinetic models can be expressed as

$$\log(q_e - q_t) = log q_e - k_1 t/2.303 \quad \ldots\ldots \quad (5.1)$$

$$\frac{t}{q_t} = \frac{1}{k_2 q_e^2} + \frac{t}{q_e} \quad \ldots\ldots \quad (5.2)$$

where,

q_e (mgg^{-1}) and q_t (mgg^{-1}) are the adsorption capacity at equilibrium and at time t, respectively,

k_1 (min^{-1}) is the pseudo-first order rate constant, and

k_2 ($gmg^{-1}min^{-1}$) is the pseudo-second order rate constant

The values of k_1, k_2 and q_e can be calculated from the slope and intercept of the linear plots of $\log(q_e - q_t)$ and t/q_t against t, respectively [17].

The kinetic parameters along with the correlation coefficients (R^2) are summarized in Table 5.1 and the kinetics models are shown in Figure 5.3. It is observed that R^2 values

Table 5.1 Kinetics parameters for the adsorption of CR at pH 3.0 and RhB at pH 7.0 onto SnO_2 nanostructures.[a]

Catalyst	Dye	pH	$q_{e,exp}$ (mgg^{-1})	Pseudo-1st order kinetics			Pseudo-2nd order kinetics		
				k_1 (min^{-1})	$q_{e,cal}$ (mgg^{-1})	R^2	k_2 (gmg^{-1} min^{-1})	$q_{e,cal}$ (mgg^{-1})	R^2
SnO_2 NS	CR	3.0	15.40	0.09	3.83	0.88	0.12	15.58	0.99
	RhB	7.0	13.27	0.09	3.54	0.89	0.12	13.45	0.99
SnO_2 NP	CR	3.0	12.80	0.09	3.84	0.91	0.11	12.97	0.98
	RhB	7.0	11.40	0.09	3.72	0.91	0.10	11.51	0.99

[a]Conditions: amount of mixed dye solution = 20 mL, concentration of dye solution = 3 mgL^{-1} and amount of catalyst = 3 mg.

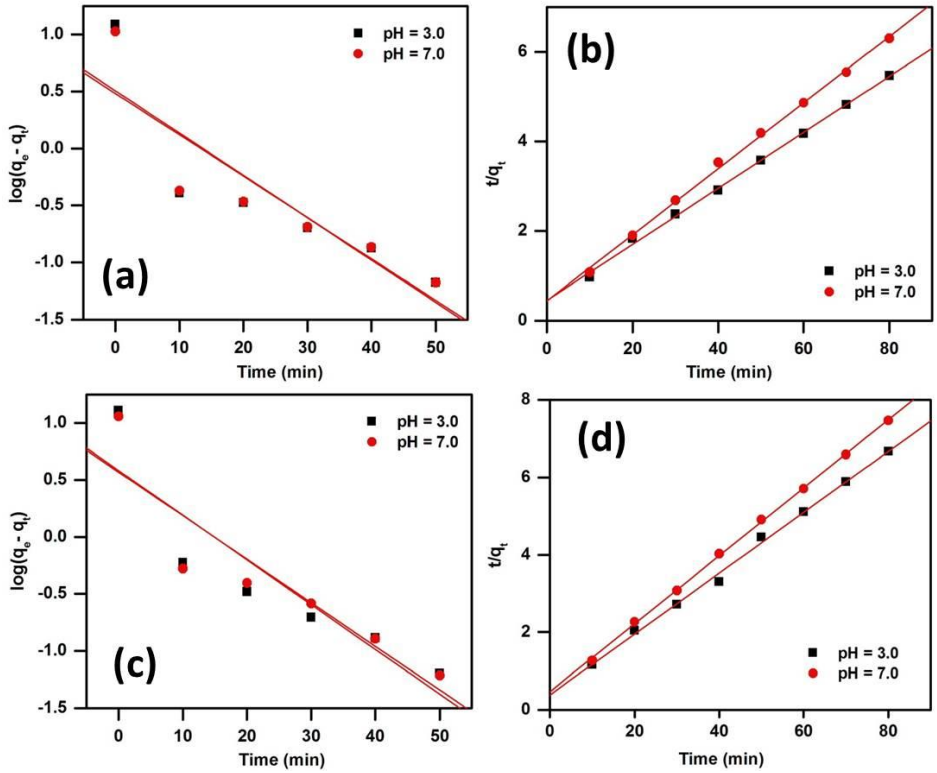

Figure 5.3 Pseudo-first order and pseudo-second order kinetics model for adsorption of CR-RhB mixed dye solution onto SnO_2 NS (a, b) and SnO_2 NP (c, d), respectively. Conditions: amount of mixed dye solution = 20 mL, concentration of dye solution = 3 mgL^{-1} and amount of catalyst = 3 mg.

for the pseudo-second order kinetic model at pH 3.0 and 7.0 are closer to unity than for the pseudo-first order model. Furthermore, the values of experimental adsorption capacity ($q_{e,exp}$) at both pH of the pseudo-second order kinetic model are much closer to the calculated adsorption capacity ($q_{e,cal}$) than for the pseudo-first order model. These observations suggest that the pseudo-second order kinetic model fits well for the adsorption of CR and RhB onto SnO_2 surfaces surfaces at pH 3.0 and 7.0, respectively.

5.2.2.3 Adsorption isotherms

The adsorption isotherms provide information on the adsorption capacity of adsorbent and the interaction between the absorbent (SnO_2 nanostructures) and the adsorbate (CR and RhB dyes) when the adsorption reaches equilibrium. Two models, Langmuir and Freundlich models are considered to investigate the representative dyes (CR and RhB) adsorption onto SnO_2 surface. According to the Langmuir model, there is no interaction between adsorbed molecules and adsorption can occur over homogeneous adsorbent surface sites, i.e., all sorption sites are identical and energetically equivalent [18, 19]. However, Freundlich isotherm describes non ideal adsorption or adsorption over heterogeneous surface system with inconsistent sorption heat distribution. The linearized forms of the Langmuir (equation 5.3) and Freundlich (equation 5.4) adsorption isotherms are expressed as

$$\frac{C_e}{q_e} = \frac{C_e}{q_m} + 1/q_m K_L \qquad \ldots\ldots \quad (5.3)$$

$$lnq_e = \left(\frac{1}{n}\right) lnC_e + lnK_F \qquad \ldots\ldots \quad (5.4)$$

where,

C_e denotes the equilibrium concentration (mgL^{-1}) of dye,

q_e (mgg^{-1}) and q_m (mgg^{-1}) correspond to equilibrium and maximum adsorption capacity of the adsorbent, and

K_L and K_F are the Langmuir and Freundlich constants.

The values of q_m and K_L can be obtained from the slope and intercept of the linear plot of C_e/q_e versus C_e. The values of K_F and n can be calculated from the intercept and slope of the linear plot of ln q_e against ln C_e. n denotes the adsorption intensity where $n > 1$ is indicative of a favorable condition for adsorption. Both the isotherm models at pH 3.0

and 7.0 based on the experimental studies are presented in Figure 5.4 and 5.5 and the relative parameters as well as correlation coefficients are reported in Table 5.2.

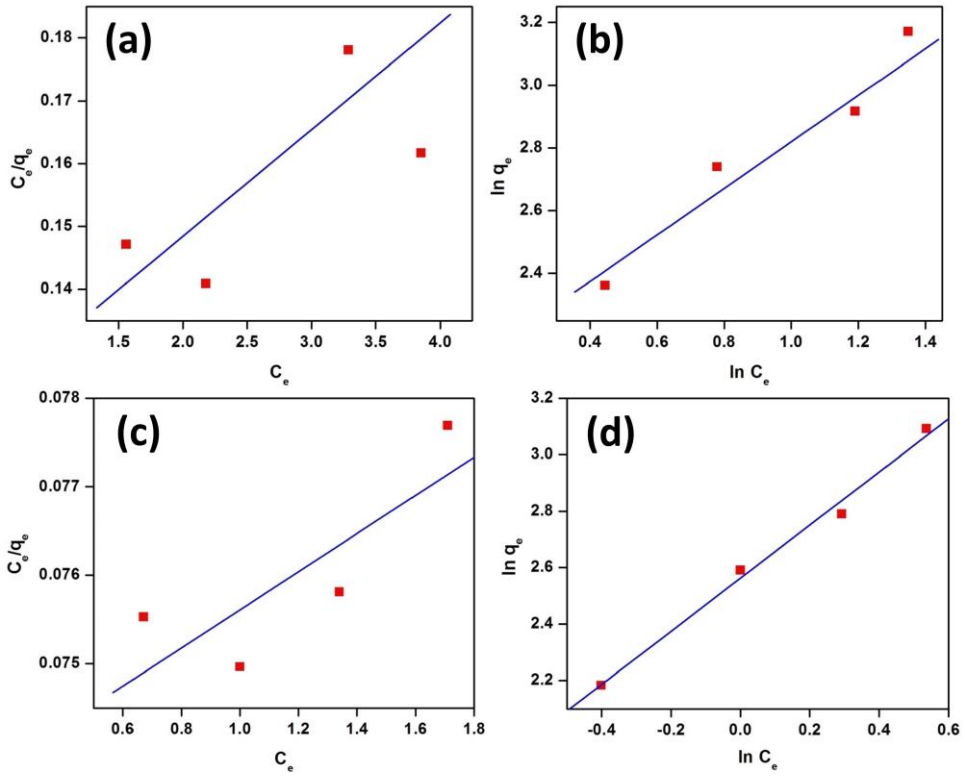

Figure 5.4 Langmuir and Freundlich adsorption isotherm model for adsorption of CR-RhB mixed dye solution onto SnO_2 NS at pH 3.0 (a, b) and 7.0 (c, d), respectively. Conditions: amount of mixed dye solution = 20 mL and amount of catalyst = 3 mg.

Table 5.2 Isotherm parameters for the adsorption of CR and RhB by SnO_2 nanocatalysts at pH 3.0 & 7.0, respectively.[a]

Catalyst	Dye	pH	Langmuir Isotherm			Freundlich Isotherm		
			q_m (mgg^{-1})	K_L (Lmg^{-1})	R^2	K_F	n	R^2
SnO_2 NS	CR	3.0	86.36	0.10	0.29	7.99	1.39	0.94
	RhB	7.0	462.96	0.03	0.50	13.23	1.02	0.99
SnO_2 NP	CR	3.0	55.04	0.11	0.71	5.78	1.33	0.95
	RhB	7.0	434.78	0.02	0.28	9.31	1.02	0.98

[a]Conditions: amount of mixed dye solution = 20 mL and amount of catalyst = 3 mg.

A better fit of the Freundlich isotherm in all the cases reveals that an adsorption over heterogeneous surface system has taken place for the present study.

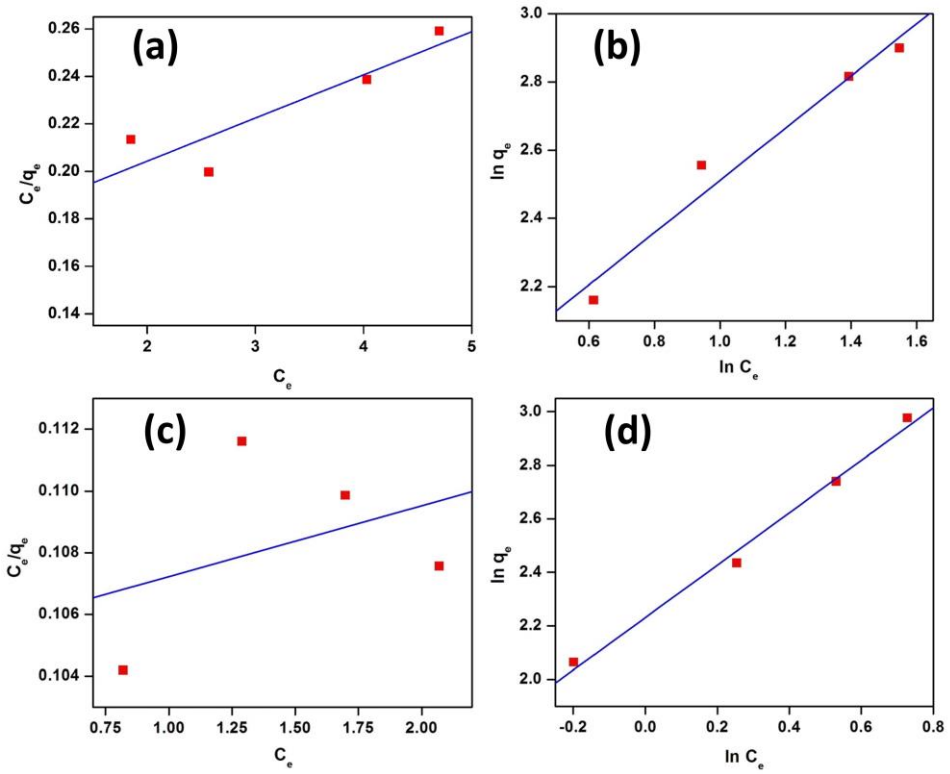

Figure 5.5 Langmuir and Freundlich adsorption isotherm model for adsorption of CR-RhB mixed dye solution onto SnO_2 NP at pH 3.0 (a, b) and 7.0 (c, d), respectively. Conditions: amount of mixed dye solution = 20 mL and amount of catalyst = 3 mg.

5.2.2.4 Effect of pH

The pH of solution is one of the most significant parameters in defining an adsorbent's adsorption characteristics since it can alter the net charge on the adsorbent as well as the adsorbate [20–22]. Figure 5.6 displays the effect of pH of the solution on the adsorption of CR−RhB mixture onto SnO_2 nanostructures in the pH range 2.0–11.0. After adsorption, the dye concentration at different pH values is measured using UV-visible spectrophotometer at two different wavelengths, viz., 497 (λ_{max} of CR) and 554 (λ_{max} of RhB) nm. At 497 nm, the adsorption capacity of SnO_2 nanostructures is increasing in acidic medium and reaches maximum at pH = 3.0, thereafter remain constant, which is similar to previously reported result for removal of anionic dyes [20]. It is important to note that the initial pH value of the mixture of the dyes solution is ~7.0 (neutral). At 554 nm, it is observed that adsorption capacity of SnO_2 nanocatalysts in basic medium almost remain constant up to pH=7, whereas in acidic medium, the adsorption capacity declined sharply. Therefore, we did not alter the pH of the mixture of dyes solution for removal of RhB. However, the adsorption capacity of SnO_2

nanocatalysts for removal of cationic dye not increasing constantly with increasing pH cannot be explained accurately by the electrostatic interaction of RhB, a cationic dye with the adsorbate's surface [21]. Therefore, other mechanism such as electron-donor-acceptor interaction and pore-filling may be favorable for the removal of RhB [22]. Finally, the results suggest that the adsorbent can significantly remove CR at pH 3.0 whereas it can remove RhB at pH 7.0 from the mixture of CR−RhB solution.

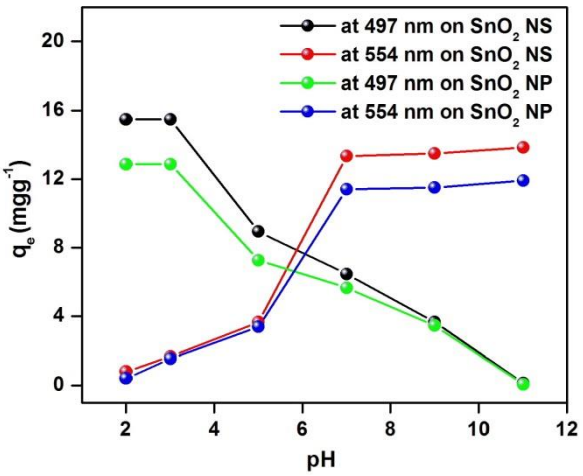

Figure 5.6 Effect of pH on adsorption of CR-RhB mixed dye solution at 497 and 554 nm onto SnO_2 nanostructures. Conditions: amount of mixed dye solution = 20 mL, concentration of dye solution = 3 mgL^{-1} and amount of catalyst = 3 mg.

5.2.2.5 Adsorption mechanism

To understand the adsorption phenomenon to a deeper extent, FTIR analysis are performed for the SnO_2 samples before and after CR-RhB adsorption (Figure 3B.1a and Figure A.2a & A.9 of Appendix). The spectra of the oxide samples show some remarkable changes after adsorption of both dyes onto its surface. Apart from the parent peaks of SnO_2, some new peaks are located at 1120.6, 1365.4 and 1607.4 cm^{-1} corresponding to CH_3, C–N and N=N groups of both the dyes. The peaks at 816.4 and 868.5 cm^{-1} corresponding to C–H bond of substituted benzene ring has been observed in case of CR-RhB adsorbed SnO_2 samples [23]. This indicates that CR and RhB dyes are successfully adsorbed onto the surface of the SnO_2 samples during the adsorption.

Again, oxide surfaces are usually covered with hydroxyl groups (acid and base) generated via the dissociative chemisorption of H_2O molecules [24]. It is known that a base hydroxyl group gets protonated, resulting in a positive site, $SnOH_2^+$ (equation 5.5)

$$\equiv SnOH(b) + H_2O \quad \rightleftharpoons \quad \equiv SnOH_2^+ + OH^- \qquad \ldots\ldots (5.5)$$

wherein $R{-}SO^{3-}$ and Cl^- are electrostatically adsorbed from CR and RhB, respectively. Again, an acid hydroxyl group gets dissociated into an H^+ ion and results in a negative site, SnO^- (equation 5.6) to which $R{-}N^+$ and Na^+ are electrostatically adsorbed from

$$\equiv SnOH(a) \quad \rightleftharpoons \quad \equiv SnO^- + H^+ \qquad \ldots.. (5.6)$$

RhB and CR, respectively. However, equation 5.6 is constrained at pH 3.0 because of the acidic property of catalytic system and at the same time the reaction 5.5 is favoured [27]. Similarly, equation 5.6 is comparably favoured at pH 7.0 than the reaction 5.5 and other mechanism like Lewis acid-base and pore-filling can also be beneficial for the adsorption of RhB [25]. Therefore, the adsorption of CR onto the nanostructures is favored at pH 3.0, whereas RhB at pH 7.0. However, some extent of adsorption of CR and RhB occur at pH 7.0 and 3.0, respectively on account of the interaction of oxygen and nitrogen atoms in the $R{-}SO_3^-$ ions (of CR) and $R{-}N^+$ ions (of RhB) with Sn^{4+} cations through a weak Lewis acid−base reaction [24, 25]. Consequently, the SnO_2 nanocatalysts can remarkably remove CR and RhB at pH 3.0 and 7.0, respectively, which is also confirmed by the results obtained in Figure 5.5.

5.2.2.6 Reusability test

Regeneration/reusability of adsorbent material is a vital aspect for practical applications. To check the reusability of the synthesized SnO_2 adsorbents, five consecutive adsorption−desorption cycles are performed at pH 3.0 and 7.0 onto SnO_2 NS and presented in Figure 5.7. It is observed that even after five consecutive cycles, the

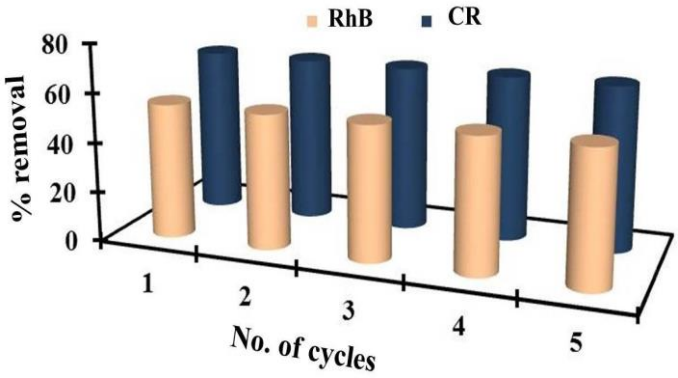

Figure 5.7 Removal efficiencies of CR and RhB at pH 3.0 & 7.0 onto SnO_2 NS in different cycles. Conditions: amount of mixed dye solution = 20 mL, concentration of dye solution = 3 mgL^{-1} and amount of catalyst = 3 mg.

removal percentage of CR and RhB from the mixed aqueous solution remains unaltered. The removal percentages of CR and RhB at the 1st adsorption−desorption cycle are 67.69 and 52.2 %, whereas after the 5th cycle, the values are 67.43 and 51.95 %, respectively. These results indicate potential adsorption capacity of the SnO_2 NS adsorbent with good reusability.

In summary, we have successfully synthesized SnO_2 nanocatalysts via a simple solvothermal route. Their adsorption capacities are investigated systematically towards the removal of CR and RhB dye selectively from their aqueous mixture. Based on the alterations of reaction parameter during the synthesis process, the surface morphology and property of the SnO_2 are changed. Therefore, they show diverse activities for the adsorption process. Moreover, the adsorption capacities of the synthesized adsorbents depend on the pH of the dye solution. At pH 3.0, it significantly removes CR (~68 % removal efficiency) owing to the interactions between the base hydroxyl group of tin dioxide and $R-SO_3^-$ ions of CR, while at pH 7.0, it selectively removes RhB up to almost 52% due to the electrostatic and electron-donor-acceptor interaction between the acid hydroxyl group of tin dioxide and $R-N^+$ ions of RhB. Therefore, the SnO_2 nanostructures can be considered as potential adsorbent for the removal of dye pollutants owing to their easy method of preparation with remarkable selectivity and reusability towards the selective dye adsorption.

REFERENCES

[1] Morin-Crini, N., Lichtfouse, E., Liu, G., Balaram, V., Ribeiro, A. R. L., Lu, Z., Stock, F., Carmona, E., Teixeira, M. R., Picos-Corrales, L. A., and Moreno-Pirajan, J. C. Worldwide cases of water pollution by emerging contaminants: a review. *Environmental Chemistry Letters*, 20(4):2311–2338, 2022.

[2] Yang, Y., Zhang, X., Jiang, J., Han, J., Li, W., Li, X., Yee Leung, K. M., Snyder, S. A., and Alvarez, P. J. Which micropollutants in water environments deserve more attention globally? *Environmental Science & Technology*, 56(1):13–29, 2021.

[3] Ismail, M., Akhtar, K., Khan, M. I., Kamal, T., Khan, M. A., M Asiri, A., Seo, J., and Khan, S. B. Pollution, toxicity and carcinogenicity of organic dyes and their catalytic bio-remediation. *Current Pharmaceutical Design*, 25(34):3645–3663, 2019.

[4] Katheresan, V., Kansedo, J., and Lau, S. Y. Efficiency of various recent wastewater dye removal methods: A review. *Journal of Environmental Chemical Engineering*, 6(4):4676–4697, 2018.

[5] Selvaraj, V., Karthika, T. S., Mansiya, C., and Alagar, M. An over review on recently developed techniques, mechanisms and intermediate involved in the advanced azo dye degradation for industrial applications. *Journal of Molecular Structure*, 1224:129195, 2021.

[6] Santhosh, C., Velmurugan, V., Jacob, G., Jeong, S. K., Grace, A. N., and Bhatnagar, A. Role of nanomaterials in water treatment applications: A review. *Chemical Engineering Journal*, 306:1116–1137, 2016.

[7] Behera, M., Nayak, J., Banerjee, S., Chakrabortty, S., and Tripathy, S.K. A review on the treatment of textile industry waste effluents towards the development of efficient mitigation strategy: An integrated system design approach. *Journal of Environmental Chemical Engineering*, 9(4):105277, 2021.

[8] Samsami, S., Mohamadizaniani, M., Sarrafzadeh, M. H., Rene, E. R., and Firoozbahr, M. Recent advances in the treatment of dye-containing wastewater from textile industries: Overview and perspectives. *Process Safety and Environmental Protection*, 143:138–163, 2020.

[9] Shabir, M., Yasin, M., Hussain, M., Shafiq, I., Akhter, P., Nizami, A. S., Jeon, B. H., and Park, Y. K. A review on recent advances in the treatment of dye-polluted wastewater. *Journal of Industrial and Engineering Chemistry*, 112:1–19, 2022.

[10] Cheng, Z., Liao, J., He, B., Zhang, F., Zhang, F., Huang, X., and Zhou, L. One-step fabrication of graphene oxide enhanced magnetic composite gel for highly efficient dye adsorption and catalysis. *ACS Sustainable Chemistry & Engineering*, 3(7):1677–1685, 2015.

[11] Geng, Z., Lin, Y., Yu, X., Shen, Q., Ma, L., Li, Z., Pan, N., and Wang, X. Highly efficient dye adsorption and removal: a functional hybrid of reduced graphene oxide–Fe_3O_4 nanoparticles as an easily regenerative adsorbent. *Journal of Materials Chemistry*, 22(8):3527–3535, 2012.

[12] Moosavi, S., Lai, C. W., Gan, S., Zamiri, G., Pivehzhani, O. A., and Johan, M. R. Application of efficient magnetic particles and activated carbon for dye removal from wastewater. *ACS Omega*, 5(33):20684–20697, 2020.

[13] Tan, I. A. W., Ahmad, A. L., and Hameed, B. H. Adsorption of basic dye on high-surface-area activated carbon prepared from coconut husk: Equilibrium, kinetic and thermodynamic studies. *Journal of Hazardous Materials*, 154(1-3):337–346, 2008.

[14] Javed, H., Luong, D. X., Lee, C. G., Zhang, D., Tour, J. M., and Alvarez, P. J. Efficient removal of bisphenol-A by ultra-high surface area porous activated carbon derived from asphalt. *Carbon*, 140:441–448, 2018.

[15] Crini, G., Lichtfouse, E., Wilson, L. D., and Morin-Crini, N. Conventional and non-conventional adsorbents for wastewater treatment. *Environmental Chemistry Letters*, 17:195–213, 2019.

[16] Ali, M. E., Hoque, M. E., Safdar Hossain, S. K., and Biswas, M. C. Nanoadsorbents for wastewater treatment: next generation biotechnological solution. *International Journal of Environmental Science and Technology*, 17:4095–4132, 2020.

[17] Weber, W. J. and Morris, J. C. Kinetics of adsorption on carbon from solution. *Journal of the Sanitary Engineering Division*, 89:31–60, 1963.

[18] Langmuir, I. The constitution and fundamental properties of solids and liquids. Part I. Solids. *The Journal of American Chemical Society*, 38(11):2221–2295, 1916.

[19] Freundlich, H. M. F. Uber die adsorption in losungen. *Zeitschrift fur Physikalische Chemie-Leipzig*, 57(A):385–470, 1906.

[20] Vimonses, V., Lei, S., Jin, B., Chow, C. W., and Saint, C. Adsorption of Congo red by three Australian kaolins. *Applied Clay Science*, 43(3-4):465–472, 2009.

[21] Kedves, E. Z., Bárdos, E., Gyulavári, T., Pap, Z., Hernadi, K., and Baia, L. Dependence of cationic dyes' adsorption upon α-MoO_3 structural properties. *Applied Surface Science*, 573:151584, 2022.

[22] Chen, X., Li, H., Liu, W., Zhang, X., Wu, Z., Bi, S., Zhang, W., and Zhan, H. Effective removal of methyl orange and rhodamine B from aqueous solution using furfural industrial processing waste: Furfural residue as an eco-friendly biosorbent. *Colloids and Surfaces A: Physicochemical and Engineering Aspects*, 583:123976, 2019.

[23] Dhanavel, S., Nivethaa, E. A. K., Dhanapal, K., Gupta, V. K., Narayanan, V., and Stephen, A. J. R. A. α-MoO_3/polyaniline composite for effective scavenging of rhodamine B, Congo red and textile dye effluent. *RSC Advances*, 6(34):28871–28886, 2016.

[24] Yang, Z., Yang, Y., Zhu, X., Chen, G., and Zhang, W. An outward coating route to CuO/MnO_2 nanorod array films and their efficient catalytic oxidation of acid fuchsin dye. *Industrial & Engineering Chemistry Research*, 53(23):9608–9615, 2014.

[25] Bauer, C., Jacques P., and Kalt, A. Investigation of the interaction between a sulfonated azo dye (AO7) and a TiO_2 surface. *Chemical Physics Letters*, 307(5–6):397–406, 1999.